2014 IEEE International Conference on Automation Science and Engineering

Workshop on Advanced Intelligent Automation Technology

Topic 7

Development of an intellectualized symmetric high-speed dual-spindle grinding machine and study on LED probe speedy grinding

Shun-Tong Chen, Ming-Jenq Twu, Chung-Yen Su, Shuen-De Wu
National Taiwan Normal University, Taiwan

Outline

Background

1. Miniaturization of products is a recent trend.
2. LED (Light Emitting Diode) is one of today's most energy-efficient and rapidly-developing lighting technologies.
3. It has the potential to fundamentally change the future of lighting all over the world.
4. Accordingly, a wear-resistant and conductive LED probe is essential for testing LED during process.

Objective

1. The objective of the research project is to develop an intellectualized symmetric high-speed dual-spindle grinding machine.
2. By applying the developed techniques of the four sub-projects, the LED-probe made of tungsten carbide can be ground efficiently.
3. The current development is focused on the feasibility study of LED-probe fast grinding with less costly way and construction of the autonomous technology.

The project team

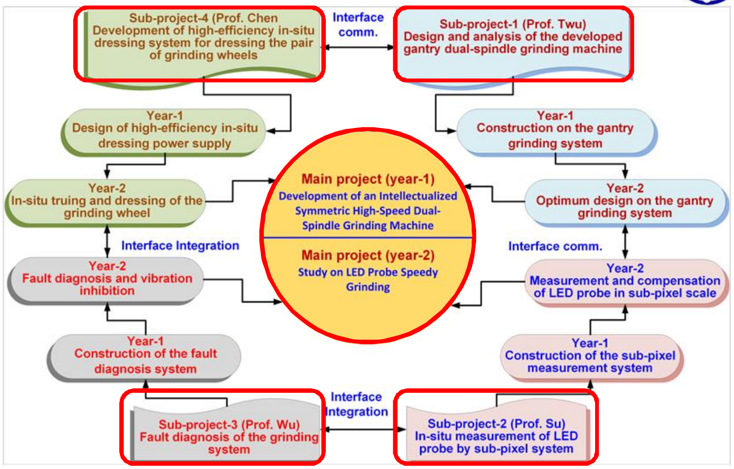

The application and design of LED probe

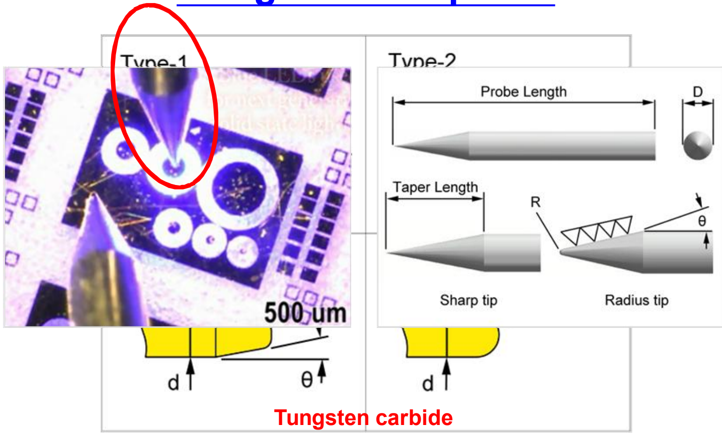

Design of the intellectualized symmetric high-speed dual-spindle grinding machine

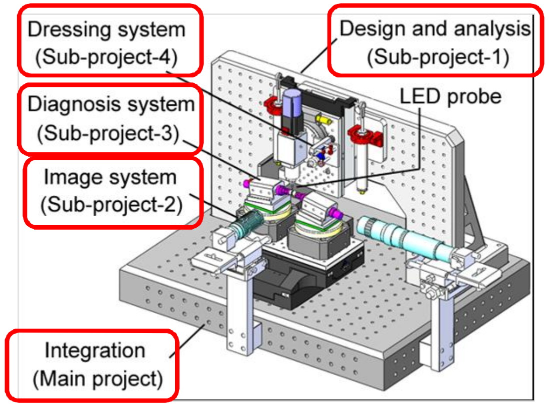

Design of the intellectualized symmetric high-speed dual-spindle grinding machine

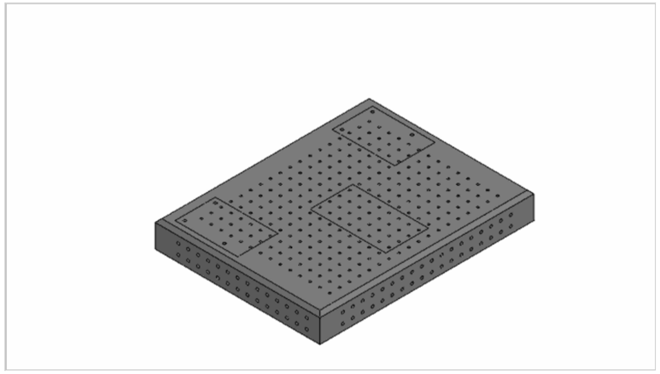

This machine is equipped with three translation stages (X-, Y- and Z-axis), one rotary stage (as the C-axis) and two high-speed dual-spindle.

Finished intellectualized symmetric high-speed dual-spindle grinding machine

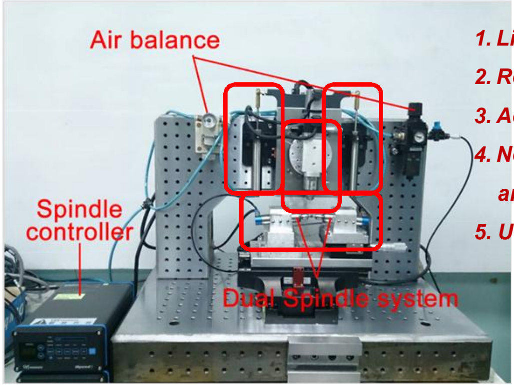

1. Linear motor (stage)
2. Resolution: 1nm
3. Accuracy: +/- 300nm
4. No contact, no wear and no backlash
5. USD 300,000 totally

A nanometer scale grinding depth can be provided in the grinding system.

The proposed approach – double-grinding

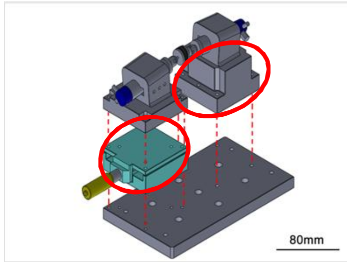

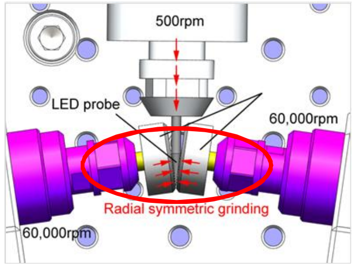

1. ***To guarantee a high-efficiency and high-precision machining on the LED probe, a double-grinding approach is proposed in this study.***
2. ***This design is helpful in increasing the bilateral symmetry and the grinding efficiency of the LED probe.***

Single-grinding

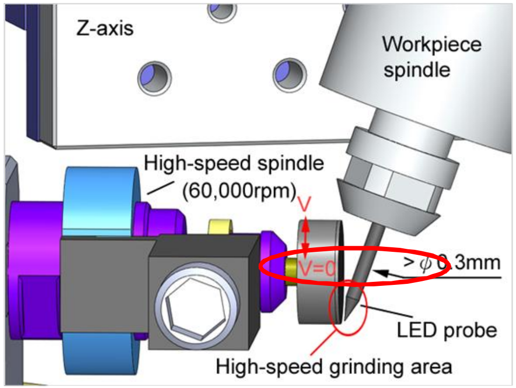

Note, the grinding area is not at the central part of the grinding-wheel since the speed of this area is zero.

The grinding-wheel used

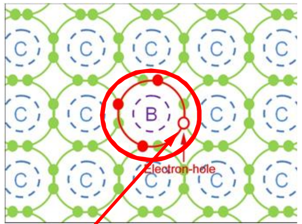

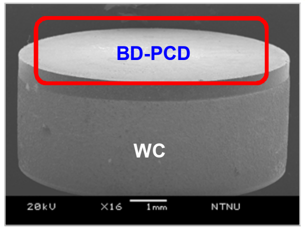

Boron-doped polycrystalline composite diamond (BD-PCD)

Electron-hole in the diamond lattice, which can contribute to electric conduction.

The BD-PCD grinding-wheel can be more easily trued by micro rotary w-EDM.

Grinding-wheel truing process

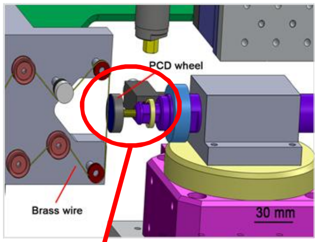

In-situ truing

Boron-doped polycrystalline composite diamond (BD-PCD)

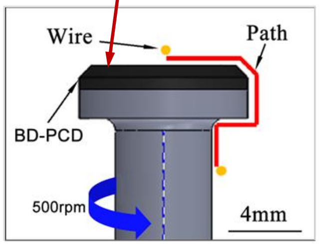

A high co-axial accuracy is achieved between the grinding-wheel and the high-speed spindle.

The BD-PCD grinding-wheel is formed by using micro rotary w-EDM.

The trued surface of the BD-PCD grinding-wheel

The trued surface

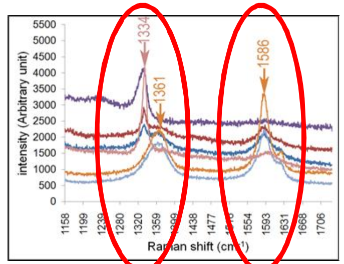

Raman spectrum

- ***During the discharge process, the temperature in the plasma channel may reach 8,000-12,000℃.***
- ***Hence, graphitizing of diamond is inevitable.***

LED-probe grinding test

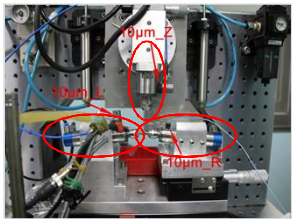

Parameter	Condition
Spindle speed	25,000-60,000(rpm)
Workpiece speed	500(rpm)
Workpiece	Tungsten carbide
Diameter	Φ0.7(mm)
Grinding depth	1(µm/stroke)
Grain size	10, 25, 40(µm)
Feed-rate	0.2(mm/min)
Coolant	DOG 1000(Oil-base)
Grinding time	18(min)

The amount of the vibration on the corresponding spindle

A grain size of 10 micrometers is used.

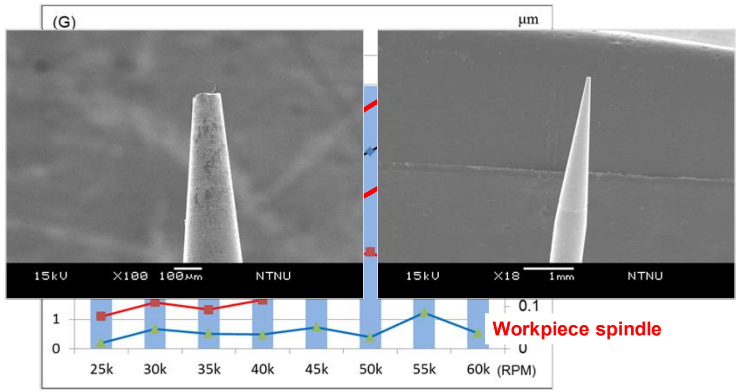

The amount of the vibration on the corresponding spindle

A grain size of 25 micrometers is used.

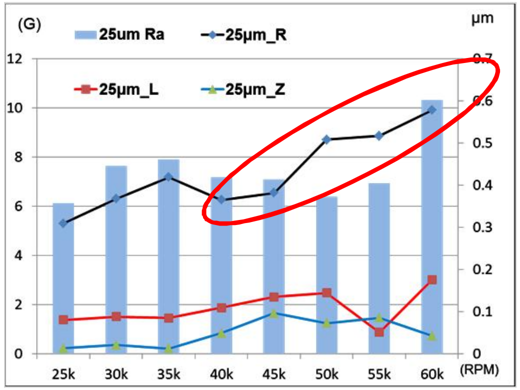

The amount of the vibration on the corresponding spindle

A grain size of 40 micrometers is used.

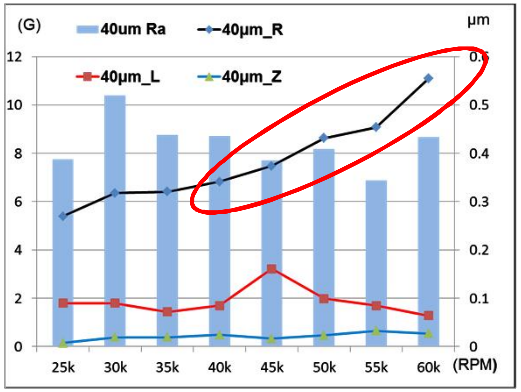

Vibration source

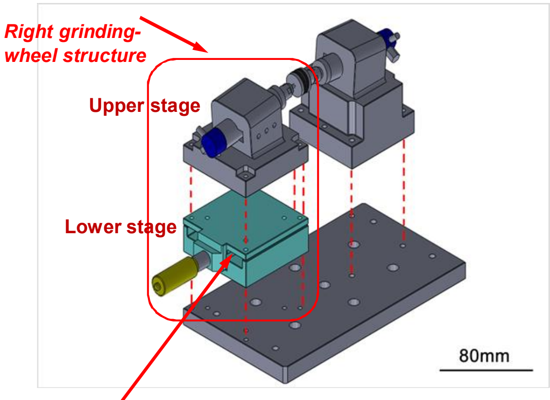

The vibration is occurred from the interface between the slide and the lower stage.

A case study in the past

(A commercial case)

Development of a quantitative cell-counting slide made of PMMA

Characteristics of urine

Composition:

Normally, a human urinary sediments are composed of about 95 percent water and 5 percent solutes.
Normal solutes found in urine include:

- Urea
- Creatinine
- Uric acid
- Ketone bodies
- Potassium
- Sodium
- Chloride

A human urinary sediments

Design of a quantitative cell-counting slide made of PMMA

(For detection of a human urinary sediments)

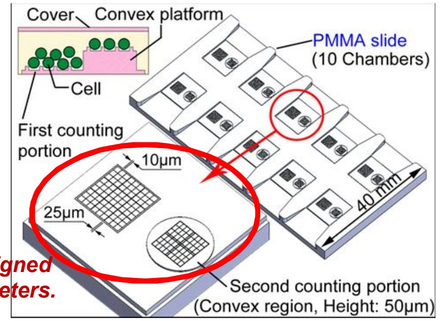

The width for each microgroove is designed only at 8-10 micrometers.

A concave platform cell-counting slide mold

The proposed in-situ fabrication process

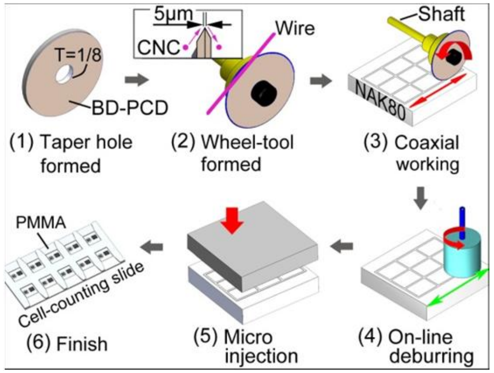

Note, in-situ fabrication enables a microgroove array to precisely generate on a biomedical-mold.

Design of the high-precision tabletop hybrid CNC machine tool

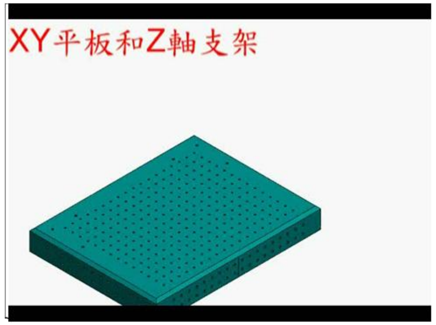

A tabletop hybrid CNC machine tool

This machine is equipped with three commercial translation stages (X-, Y- and Z- axis) and one rotary stage (as the C-axis).

Design of the perpendicular dual-spindle

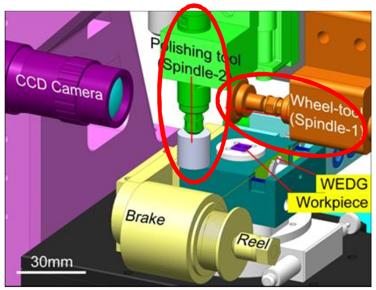

Designed dual-spindle set-up

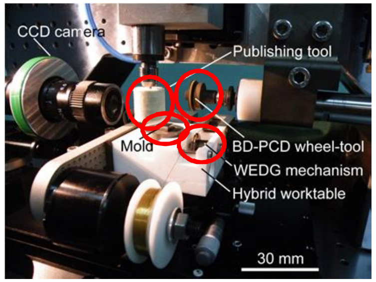

In-situ machining

To guarantee machining accuracy and reduce tedious readjustment during process, a set of perpendicular dual-spindle is propose in this study.

Analyses of deformation and resonance

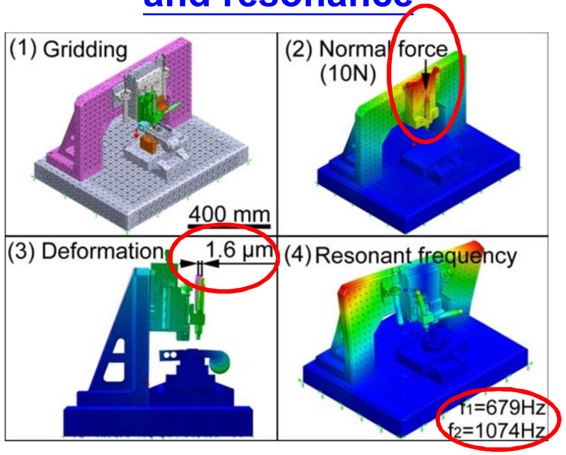

Design for the hybrid working platform

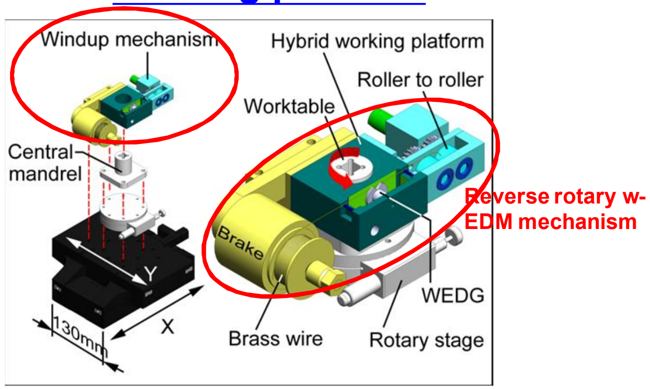

To generate the accuracy of such a fine microgroove array, a hybrid working platform to support the in-situ process is designed.

Finished tabletop hybrid CNC machine tool

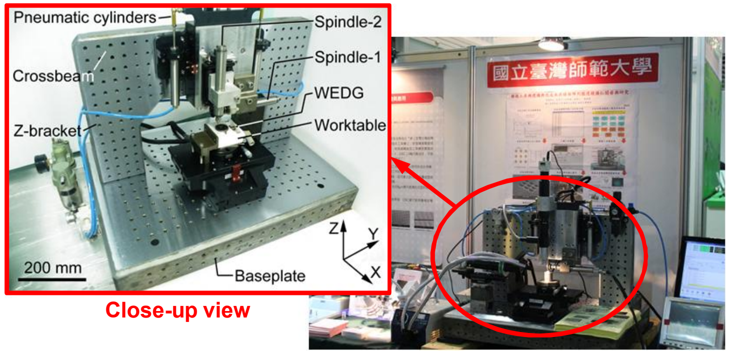

Close-up view

This machine can provide for microgroove grinding by nanometer scale grinding depth.

Thinning of the BD-PCD wheel-tool

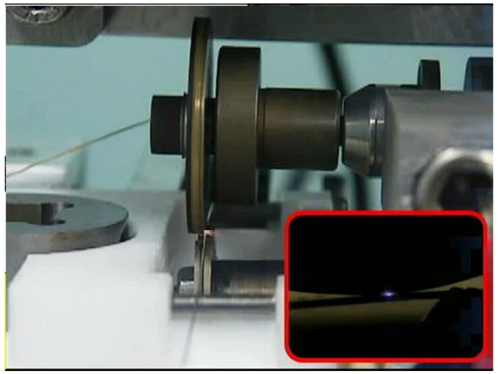

BD-PCD is capable of electrical conductivity, meaning it can be more easily cut by electrical discharge machining on the developed machine tool.

Thinned grinding-edge

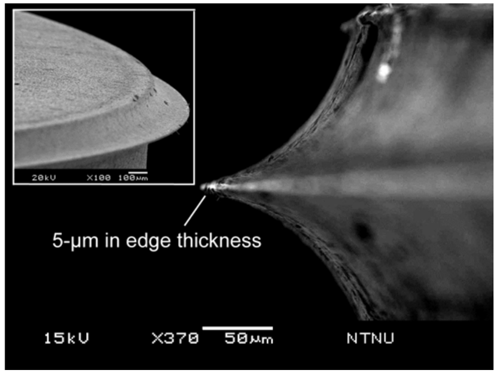

A thinned BD-PCD wheel-tool with an edge-thickness of 5-μm and a slight draft angle of 5 degree.

A smoothly cut (broken) in diamond grain

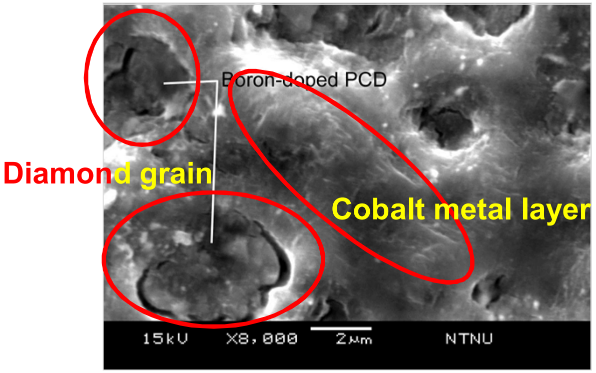

The image demonstrates the BD-PCD can be precisely formed down to an ultrathin level by rotary micro w-EDM.

Microgroove generation by HSFSG

High-Speed & Fast-Shallow Grinding

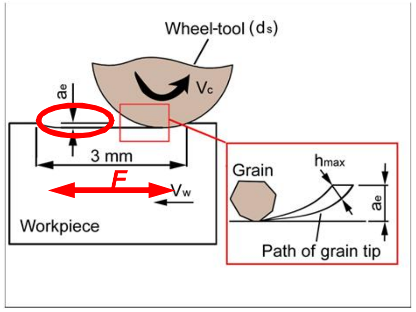

Parameters	Conditions
Spindle speed	1,500 (m/min)
Feeding depth	500 (nm/stroke)
Total feeding depth	10 (μm)
Grinding length	3 (mm)
Grinding pass	20 (One way)
Feed-rate	20 (mm/min)
Coolant	Oil mist

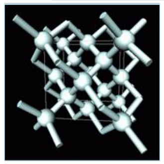

SP^3 bonds

1. **By applying a fast grinding feed-rate, we can create considerable metal removals per unit of time.**
2. **By using a nanometer scale grinding depth, we can keep the diamond lattice in SP^3 bond during grinding because of cold machining conditions used.**

Finished crisscross microgroove array

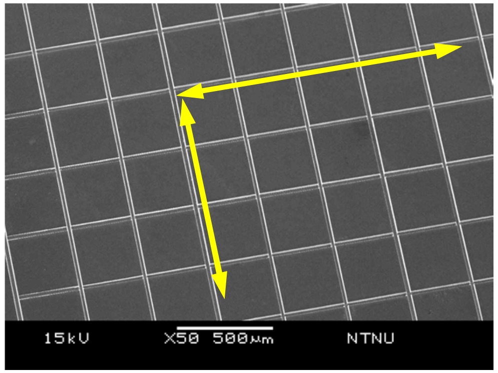

A finished microgroove array with extremely high straightness and high orthogonality.

Proposed deburring process at the intersections of microgrooves

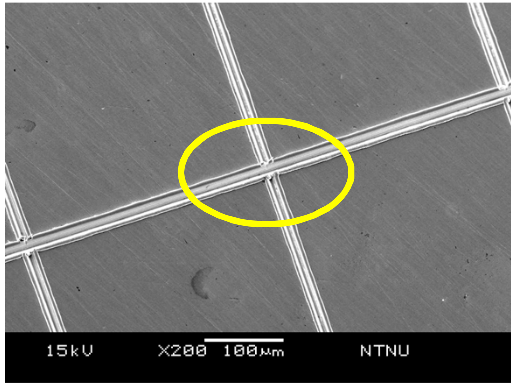

Burrs occur as a result of NAK80 mold steel being ductile, and plowing effect during microgroove grinding.

Proposed deburring process at the intersections of microgrooves(cont.)

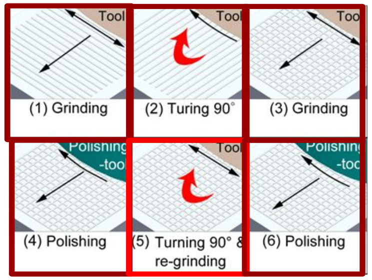

Proposed deburring process

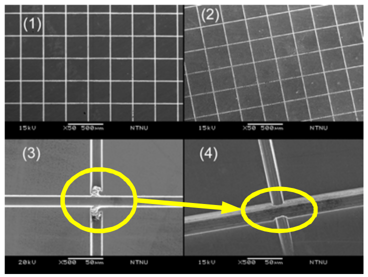

Before and after deburring

Mold design of a quantitative cell-counting slide

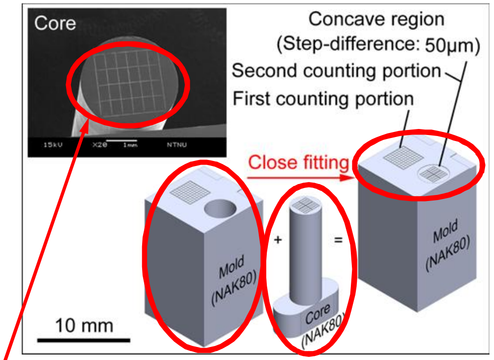

An embedded mold design approach is proposed.

The width for each microgroove is only 8-10 micrometers.

Finished cell-counting slide made of PMMA and an example of cell counting

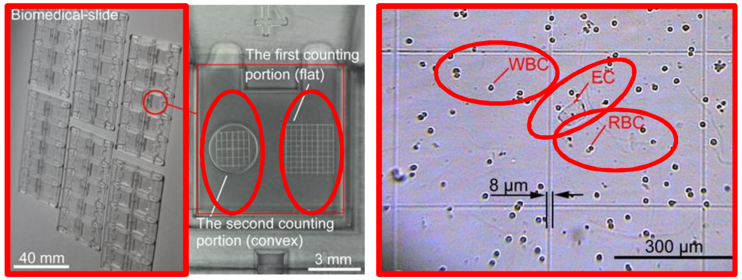

1. *Note, the two distinct cell-counting portions can be clearly revealed in each chamber.*
2. *It indicates the multiple micro ridge array of the biomedical-slide can be exactly duplicated from the machined biomedical-mold.*

Conclusions

➢ In LED probe grinding case:

1. An intellectualized symmetric high-speed dual-spindle grinding machine for LED probe grinding has been developed and verified successfully.
2. A pair of BD-PCD grinding-wheel is dressed by the rotary w-EDM and a LED probe made of tungsten carbide has been tentatively grinding in first year.

Conclusions(cont.)

➢ In biomedical-slide mold case:

1. A high-precision tabletop hybrid CNC machine tool for in-situ fabricating a biomedical-slide mold has been developed and verified successfully.
2. The High-Speed & Fast-Shallow Grinding technique is successfully used to grind microgroove array on NAK80 mold steel.
3. By using nanometer scale grinding depth results in a cold machining and preservation for diamond's SP^3 bond structure.

Conclusions(cont.)

4. Due to the design of the in-situ machining function, the machined biomedical-slide mold requires no unloading, reloading and calibration.
5. Experimental results prove the convex platform quantitative cell-counting slide is successfully developed.

Thank you so much for your attention!

2014 IEEE International Conference on Automation Science and Engineering

Workshop on Advanced Intelligent Automation Technology

Topic 7

Development of an intellectualized symmetric high-speed dual-spindle grinding machine and study on LED probe speedy grinding

Sub-project I

Design and analysis of the developed gantry dual-spindle grinding machine

Shun-Tong Chen, Ming-Jenq Twu, Chung-Yen Su, Shuen-De Wu
National Taiwan Normal University, Taiwan

Outline

1. Introduction and the objectives.
2. The proposed approach and procedures
3. Static and dynamic analysis of initial design
4. Metamodel and structural optimization
5. Summary and conclusion
6. References

Introduction

One of key issue in mechanical manufacturing is vibration [1] .

texture caused by chatter in turning

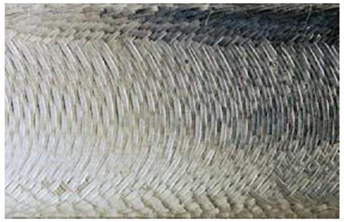

texture caused by chatter in milling

Source of figures: http://74.220.207.117/~horvathl/m-tool-vib.htm

http://www.hv.se/extra/pod/?action=pod_show&id=753&module_instance=11

Introduction

Stiffness is a key parameter of vibration problem.
The equation of 1 DOF mass-spring-damper system

$$m\ddot{x} + c\dot{x} + kx = f(t)$$

$$\omega_n = \sqrt{\frac{k}{m}}, \zeta = \frac{c}{2\sqrt{km}}, \omega_d = \omega_n\sqrt{1-\zeta^2}, \zeta < 1$$

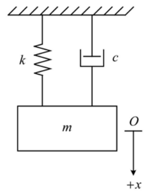

The stiffness of system is determined by mass distribution of structure.
Structural design is the foundation for the development of high-precision manufacturing system.
Analyzing stiffness is an important issue in machine tool design [2].

Objectives of sub-project I

1. To optimize the structural design for the proposed intellectualized symmetric high-speed dual-spindles grinding machine.
2. To propose a dynamic model of grinding chatter for the designed system.
3. To develop the strategy of chatter suppression for the designed system.

Procedure of research

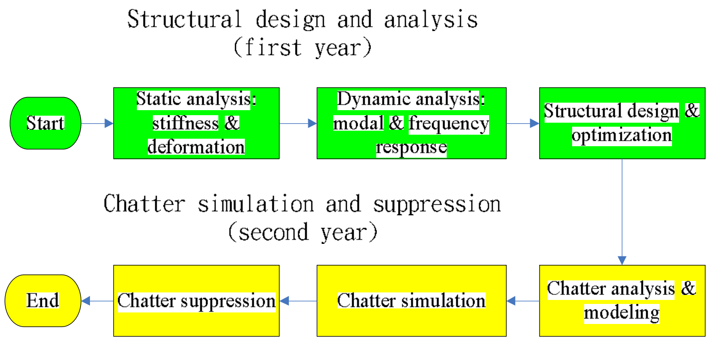

Procedure of the first year research

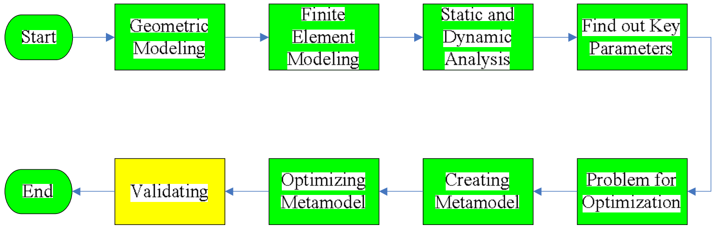

Finite element model of initial design

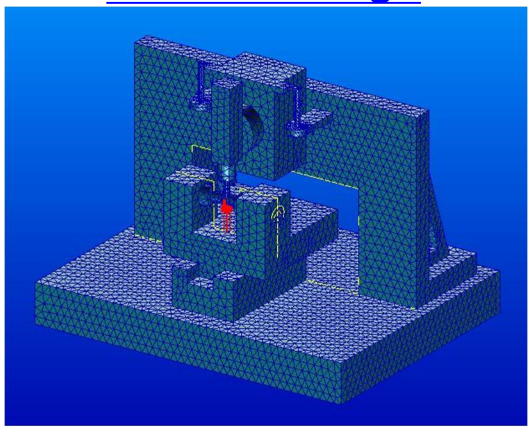

Static analysis results of initial design - displacement

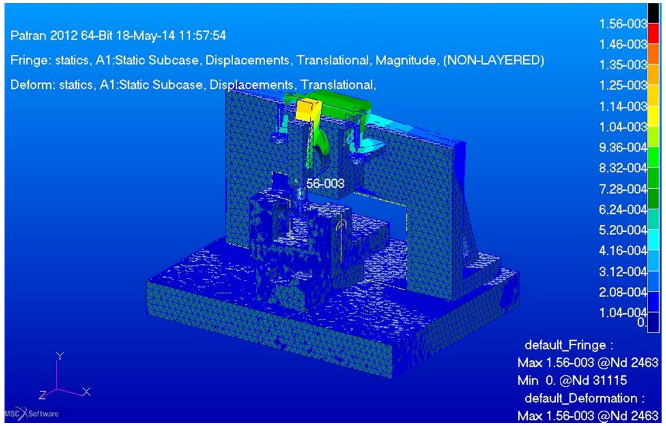

Static analysis results of initial design - stress

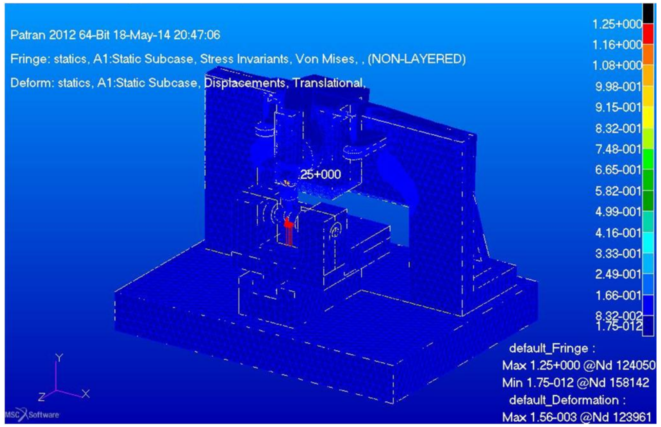

Dynamic analysis results of initial design – 1st mode

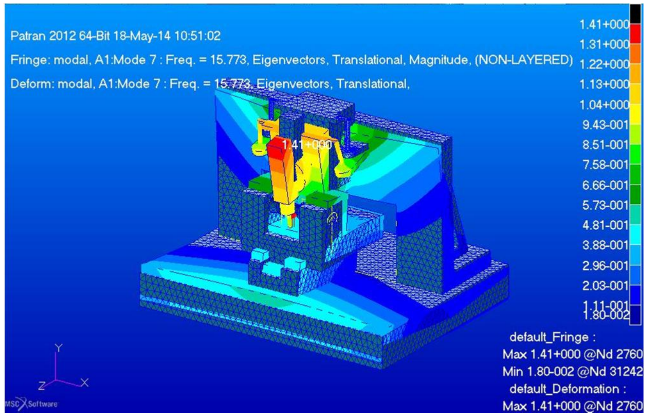

Dynamic analysis results of initial design – 2nd mode

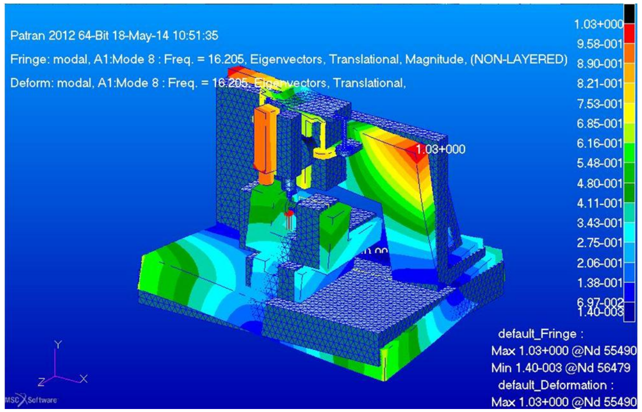

Results of analysis

Deformation at tip < 1 um

Max. stress < 2 N/mm^2

Natural frequency = 11.5, 16.2, 20, 25.1, 26.4, 38.9, 43.1, 46.7, 49.3, 50.7…

The lowest frequency > 10 Hz > the frequency of the low speed spindle (500 rpm)

The high speed spindle (60000 rpm) is far beyond the 100th natural frequency of the system.

The key part and key point of structural design

From the results of finite element analysis, the first modal shape and deformation, we know that **headstock and supporting pneumatic cylinder** play main role in static and dynamic responses.

Two key factors decide the static and dynamic behavior of the designed structure:

The **stiffness of contact interface** between headstock and column

The **coefficients of structural damping**

Optimization problem

Objective: minimize the weight (or volume)

Design variables: length (xL), height (yH), width (zW)

Constrains: deformation at tip of probe < 2 um

stress < yielding stress

2nd natural frequency > 10

(since the 2nd natural frequency is the most sensitive one)

Design Variables

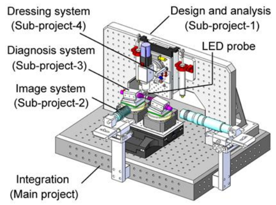

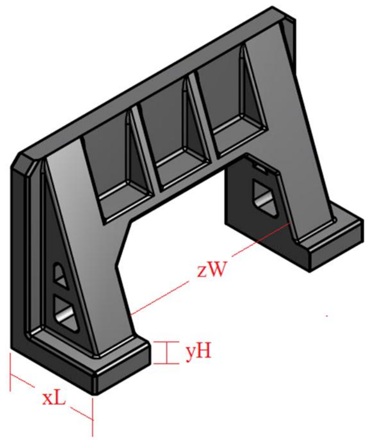

Flowchart of optimization

Mathematica: the mathematic software to do the RSM and optimization.

MSC.Patran/Nastran: the software to do the finite element analysis.

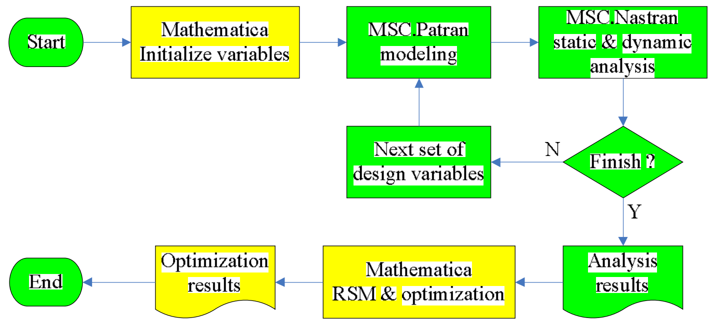

Metamodel
Response Surface Method

Metamodel

also known as surrogate model, is an approximate representation [3].

an alternative to costly analysis or experiment [4].

e.g. Genetic algorithms, artificial neural networks,…

Response surface methodology (RSM)

mathematical and statistical techniques to develop

functional relationship between input and response [5].

Design optimization is a computation intensive process.

Response surface

The **response surface** is represented by the polynomial function **F(x,y,z).**

Quadratic polynomial items for response surface

$$\{1, x, y, z, xy, xz, yz, x^2, y^2, z^2\}$$

Cubic polynomial item for response surface

$$\{1, x, y, z, xy, xz, yz, x^2, y^2, z^2, xyz, xy^2, xz^2, x^2y, x^2z, yz^2, y^2z\}$$

The process of RSM is to find the **coefficients** of these polynomial items.

Creation of response surface

Three factors, xL, yH, and zW, are used for RSM.

Three levels for each of these factors.

Totally there are 3^3 designs.

Two kinds of finite element analysis, static and dynamic analysis, are run for each design, which means 54 runs of analysis.

Two results of finite element analysis, displacement and 2nd frequency are used to create the response surface, along with volume of structure.

The stress result is not considered since it is far below the yielding stress.

Response surface of volume

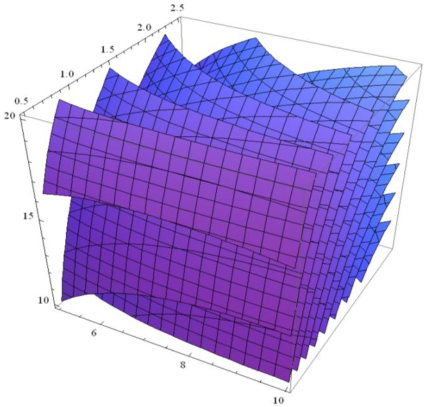

Response surface of displacement

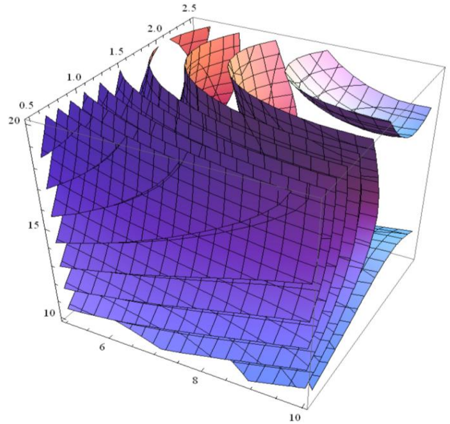

Response surface of 2nd frequency

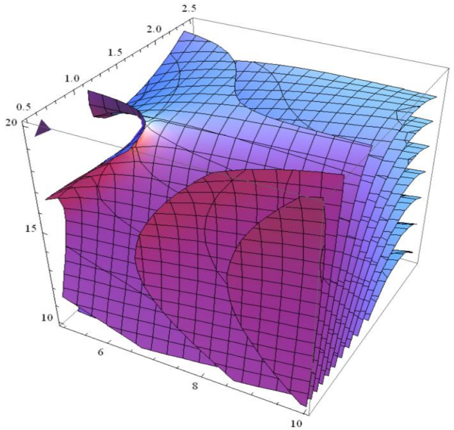

Optimization results

Mathematica is used to find the optimal point on the response surface. Quadratic and cubic polynomials are used for design I and II respectively.

	(xL, yH, zW) (mm)	Change of Volume %	Change of Displacement %	Change of Frequency %
Original Design	(200,40,355)	0	0	0
Optimal Design I	(175,51,389)	-11.34	-0.3	-0.818
Optimal Design II	(184,47,389)	-11.62	-0.32	-0.823

Summary and conclusion

The finite element analysis of initial design is used to decide the key points for subsequent analysis and design.

The optimization for the weight of structure of initial design is completed.

Metamodel with response surface method is used for optimization.

Stiffness of contact interface and structural damping coefficient of the headstock are the key parameters of analysis.

Further experiments to identify system parameters are needed for validation of the design model.

References

[1] G. P. Zhang, Y.M. Huang, W.H. Shi, W.P. Fu, Predicting dynamic behaviours of a whole machine tool structure based on computer-aided engineering, International Journal of Machine Tools & Manufacture 43, p. 699-706, 2003.

[2] D. T. Huang, J.-J. Lee, On obtaining machine tool stiffness by CAE techniques, Intl' J. of Machine Tools & Manufacture 41, p. 1149-1163, 2001.

[3] M. Ramu, V. P. Raja, P. R. Thyla, M. Gunaseelan, Design optimization of complex structures using metamodels, Jordan Journal of Mechanical and industrial Engineering, v.4 no. 5, p. 653-664, 2010.

[4] D. J. Lizotte, R. Greiner, D. Schuurmans, An experimental methodology for response surface optimization methods, Journal of Global Optimizaation, 53(4), p. 699-736, 2011.

[5] S. Chakraborty, A. Sen, Adaptive response surface based efficient finite element model updating, Finite Elements in Analysis and Design, 80, p. 33-40, 2014.

Thanks for listening

Sub-pixel Edge Detection of LED Probes Based on Partial Area Effect and Iterative Curve Fitting

Advisor：Chung-Yen Su
Students：Nai-Kuei Chen, Chen-Chun Wang, Li-An Yu

Introduction (1/2)

- This subproject is focused on measure the angle and radius of a LED probe by computer vision.
- To do that, we need to find edge points.
- Some of the common pixel-level edge detection methods are
  - Sobel, Canny, Laplacian of Gaussian (LOG), Scharr
- Sub-pixel edge detection is used to increase the precision of edge detection.
- The common sub-pixel edge detections include
  - Curve-fitting method
  - Moment-based method
  - Reconstructive method
  - Partial area effect method

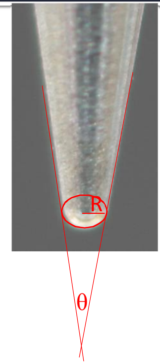

Introduction (2/2)

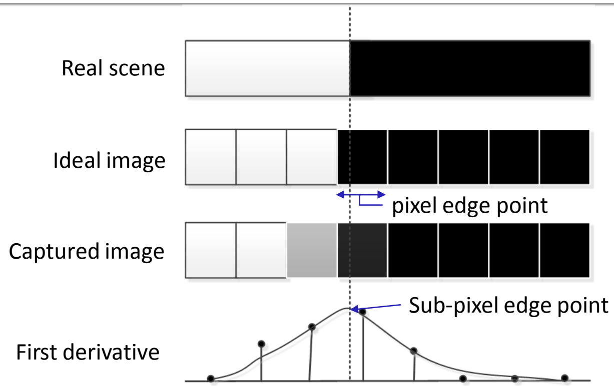

Flow Chart

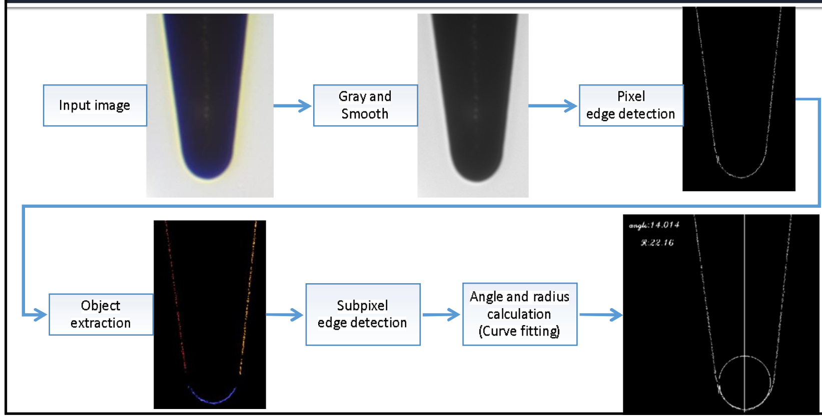

Getting the Input Image

- Yellow arrow is coaxial light from lens.

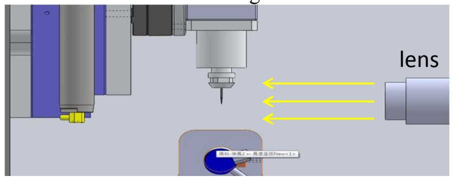

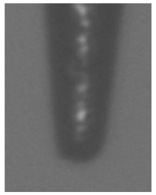

- Enhance the edge with a mirror

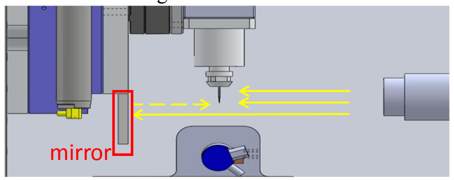

5

Converting and Smoothing

- Convert a RGB image to a gray image
  - Gray = 0.299R + 0.587G + 0.114B
- Use a Gaussian filter to smooth the resulting gray image

$\frac{1}{256}\times$

1	4	6	4	1
4	16	24	16	4
6	24	36	24	6
4	16	24	16	4
1	4	6	4	1

6

Automatic Threshold (1/2)

- For Sobel
  - Use Sobel operator to measure the magnitudes of gradient($|dx|+|dy|$) over the image and make CDF

7

Automatic Threshold (2/2)

- For Canny
  - Multiply the median of gray image by 0.3 as high threshold and 0.1 as low threshold.

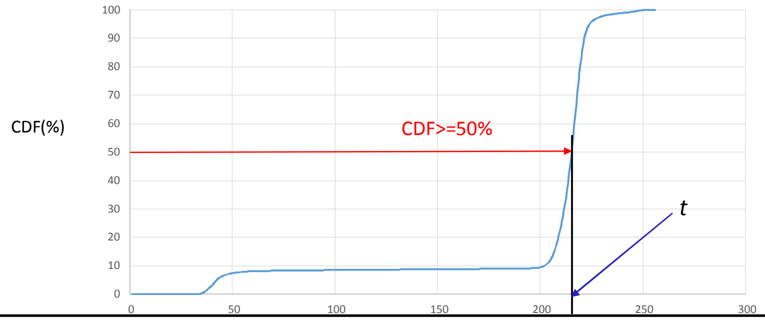

$TH_h = t \times 0.3$

$TH_l = t \times 0.1$

8

Object Extraction

- Classify edge points into three groups
  1. Distinguish between left and right side:
     $$x_{avg} = \frac{\sum_{i=0}^{edge\ point\ counts} x_i}{edge\ point\ counts}$$
  2. Get gradient direction: $\theta = \tan^{-1}\frac{dy}{dx}$

$$dx = Img * \begin{bmatrix} -1 & 0 & 1 \\ -2 & 0 & 2 \\ -1 & 0 & 1 \end{bmatrix} \qquad dy = Img * \begin{bmatrix} -1 & -2 & -1 \\ 0 & 0 & 0 \\ 1 & 2 & 1 \end{bmatrix}$$

  3. Differentiate edge points between line and circle:
     1) Line: $|\theta| < 7^{\circ}$, Circle: $|\theta| > 30^{\circ}$.
     2) Discard: $7^{\circ} \leq |\theta| \leq 30^{\circ}$

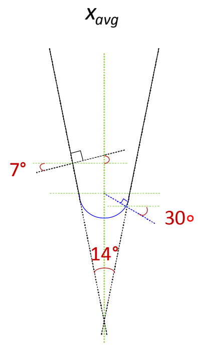

9

Sub-pixel Edge Detection

- After object extraction, we compute Sub-pixel edge detection for every groups respectively. And the Sub-pixel edge detection methods we use are:
  1. Curve-fitting method
  2. Moment-based method [1]
     - Invariant rotation and orthogonal
  3. Reconstructive method [2]
     - Create a quadratic model with adjacent gray-scale values to the selected points
  4. Partial area effect method [3]
     - Create a new mask from camera acquired images

10

Iterative Curve Fitting (1/5)

iterative times : 0

iterative times : 1

iterative times : 5

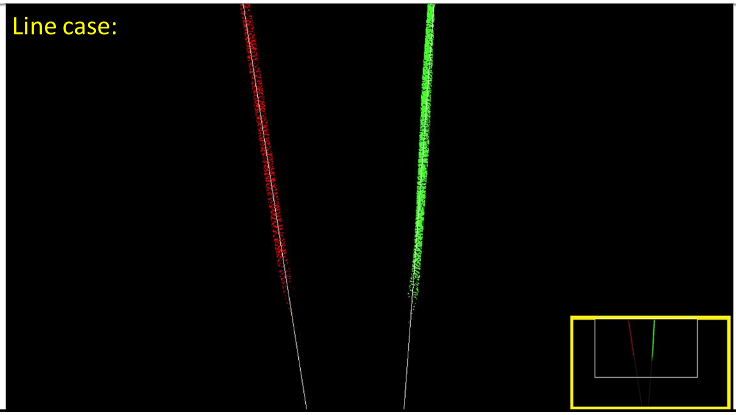

11

Iterative Curve Fitting (2/5)

Circle case:

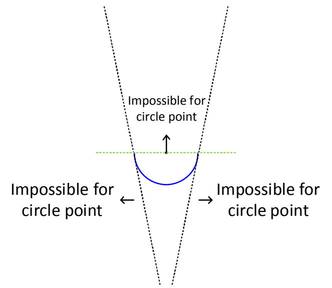

Blue line: circle points
Black line: line points

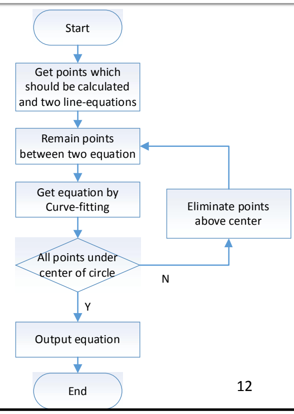

12

Iterative Curve Fitting (3/5)

iterative times : 0

iterative times : 1

iterative times : 5

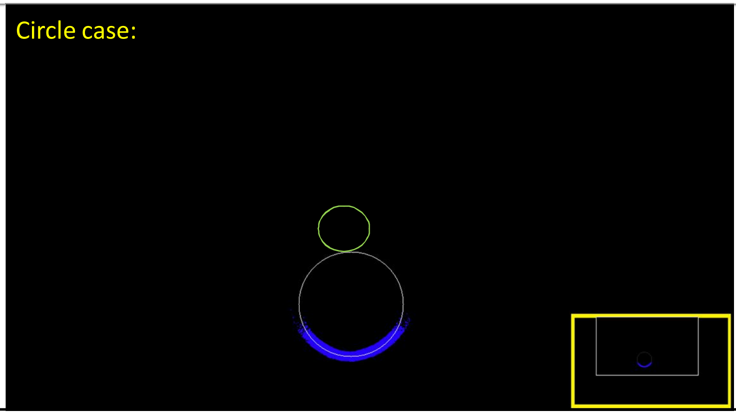

13

Iterative Curve-Fitting (4/5)

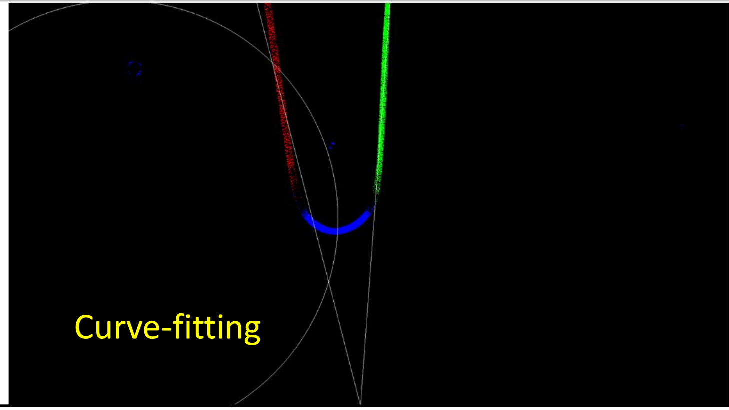

14

Iterative Curve Fitting (5/5)

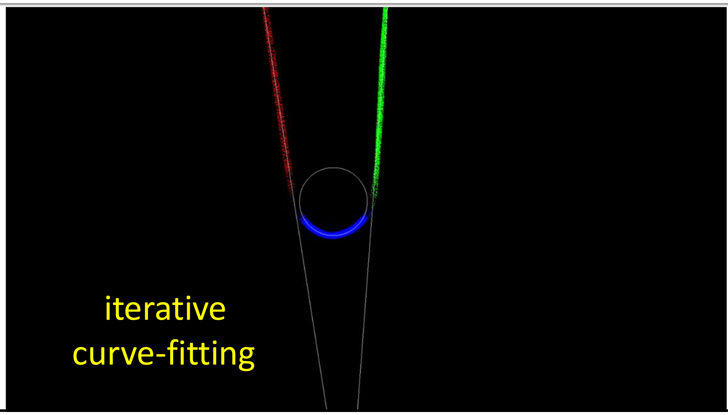

15

Calculate Angle and Radius

- Angle: Use the cosine theorem

$$\theta = \cos^{-1}\left(\left|\frac{slope_1 \times slpoe_2 + 1}{\sqrt{{slope_1}^2 + 1} \times \sqrt{{slpoe_2}^2 + 1}}\right|\right)$$

- Radius: According to parameters of circle equation

  Circular equation:

$$x^2 + y^2 + dx + ey + f = 0$$

  Radius :

$$R = \frac{1}{2}\sqrt{d^2 + e^2 - 4f}$$

16

Result

M1: Sobel + curve-fitting
M2: Sobel-Zernike moments [1] + curve-fitting
M3: Canny + curve-fitting
M4: Canny + partial area effect [3] + curve-fitting
M5: Canny + reconstructive [2] + curve-fitting

M1’: Sobel + iterative curve-fitting
M2’: Sobel-Zernike moments [1] + iterative curve-fitting
M3’: Canny + iterative curve-fitting
M4’: Canny + partial area effect [3] + iterative curve-fitting
M5’: Canny + reconstructive [2] + iterative curve-fitting

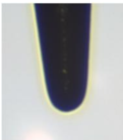

Fig. 1

Fig. 2

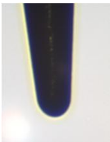

Fig. 3

Fig. 4

Fig. 5

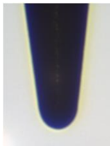

Fig. 6

17

Angle Result (1/2)

	Referred values	M1		M2		M3		M4		M5	
Angle / Image	Angle (degree)	Angle (degree)	Error(%)	Angle (degree)	Error(%)	Angle (degree)	Error(%)	Angle (degree)	Error(%)	Angle (degree)	Error(%)
Fig. 1	11	18.579	68.9	18.748	70.436	11.111	1.009	11.089	0.809	11.027	0.245
Fig. 2	11.2	11.401	1.795	11.427	2.0267	10.847	3.152	10.824	3.357	10.768	3.857
Fig. 3	9.9	13.696	38.343	13.787	39.263	10.063	1.646	10.045	1.464	10.007	1.08
Fig. 4	13.1	18.865	44.007	18.963	44.756	13.247	1.122	13.24	1.068	13.251	1.153
Fig. 5	10.8	11.411	5.657	11.433	5.861	10.824	0.222	10.816	0.148	10.803	0.027
Fig. 6	13.8	14.545	5.399	14.566	5.551	14.011	1.529	13.992	1.391	14.017	1.572
Average error		27.350%		27.982%		1.447%		1.373%		1.322%	

Angle Result (2/2)

	Referred values	M1’		M2’		M3’		M4’		M5’	
Angle / Image	Angle (degree)	Angle (degree)	Error(%)	Angle (degree)	Error(%)	Angle (degree)	Error(%)	Angle (degree)	Error(%)	Angle (degree)	Error(%)
Fig. 1	11	13.045	18.591	13.124	19.309	11.054	0.491	11.019	0.172	10.859	1.282
Fig. 2	11.2	11.457	2.295	11.486	2.554	10.826	3.339	10.801	3.563	10.749	4.027
Fig. 3	9.9	11.363	14.777	11.409	15.242	10.063	1.646	10.045	1.465	9.993	0.939
Fig. 4	13.1	14.520	10.832	14.567	11.198	13.232	1.008	13.222	0.931	13.218	0.901
Fig. 5	10.8	11.386	5.426	11.388	5.444	10.824	0.222	10.816	0.148	10.803	0.028
Fig. 6	13.8	14.545	5.399	14.566	5.551	14.011	1.529	13.992	1.391	13.982	1.319
Average error		9.553%		9.883%		1.372%		1.278%		1.416%	

Radius Result (1/2)

	Referred values	M1		M2		M3		M4		M5	
Radius / Image	Radius (um)	Radius (um)	Error(%)	Radius (um)	Error(%)	Radius (um)	Error(%)	Radius (um)	Error(%)	Radius (um)	Error(%)
Fig. 1	19.75	128.232	549.276	128.232	549.276	21.132	6.997	21.168	7.179	21.808	10.42
Fig. 2	20.25	70.994	250.588	70.995	250.592	20.512	1.294	20.529	1.378	21.472	6.035
Fig. 3	21.75	90.304	315.190	90.304	315.190	22.320	2.621	22.352	2.768	22.943	5.485
Fig. 4	22.25	134.073	502.575	134.073	502.575	23.165	4.112	23.213	4.328	22.899	2.917
Fig. 5	24.25	102.606	323.117	102.606	323.117	22.417	7.559	22.447	7.435	22.834	5.839
Fig. 6	22.75	194.681	755.741	194.681	755.741	21.976	3.402	22.014	3.235	22.385	1.604
Average error		449.415%		449.416%		4.331%		4.387%		5.383%	

Radius Result (2/2)

	Referred values	M1'		M2'		M3'		M4'		M5'	
Radius / Image	Radius (um)	Radius (um)	Error(%)	Radius (um)	Error(%)	Radius (um)	Error(%)	Radius (um)	Error(%)	Radius (um)	Error(%)
Fig. 1	19.75	20.038	1.458	20.064	1.590	21.132	6.997	21.135	7.013	21.346	8.081
Fig. 2	20.25	19.621	3.106	19.624	3.091	20.512	1.294	20.496	1.215	20.496	1.215
Fig. 3	21.75	21.330	1.931	21.318	1.986	22.320	2.621	22.335	2.689	22.574	3.788
Fig. 4	22.25	21.821	1.928	21.824	1.914	23.165	4.112	23.141	4.004	23.167	4.121
Fig. 5	24.25	21.605	10.907	21.610	10.886	22.417	7.559	22.439	7.468	22.704	6.375
Fig. 6	22.75	21.149	7.037	21.137	7.090	21.976	3.402	22.007	3.266	21.925	3.626
Average error		4.395%		4.426%		4.331%		4.276%		4.534%	

Conclusion

- According to the experiment, iterative curve-fitting normally has better results than that without iteration.
- We compare M3' with M4' because they have better results than the others:

	M3'	M4'
Run time (ms)	1473.4	1669.5
Average angle error	1.372%	1.278%
Average radius error	4.331%	4.276%

Platform: Win7 64bit, Intel Xeon E3-1230V2, 8G RAM

  - M3': Canny + iterative curve-fitting
  - M4': Canny + partial area effect [3] + iterative curve-fitting
- We use M4' as the algorithm of detecting led probes so far.

22

Reference

[1] Y. D. Qu, C. S. Cui, S. B. Chen, J. Q. Li, "A fast subpixel edge detection method using Sobel-Zernike moments operator," *Image and Vision Computing*, 23 (1), pp. 11–17, 2005.

[2] Fabija´nska, A., Sankowski, D. "Edge detection with sub-pixel accuracy in images of molten metals", *IEEE International Conference on Imaging Systems and Techniques*, Thessaloniki, Greece, pp. 186-191, 2010.

[3] A. Trujillo-Pino, K. Krissian, M. Alemán-Flores, D. Santana-Cedrés, "Accurate subpixel edge location based on partial area effect", *Image and Vision Computing*, 31, pp. 72–90, 2013.

[4] N. Q. Chen, J. J. Wang, L. A. Yu, and C. Y. Su, "Sub-pixel Edge Detection of LED Probes Based on Canny Edge Detection and Iterative Curve Fitting", in the *Proc. of IEEE International Symposium on Computer, Consumer and Control*, pp. 131-134, 2014.

23

2014 IEEE International Conference on Automation Science and Engineering

Prognostics for Rolling Bearing Based on Multiscale Entropy, Permutation Entropy and Support Vector Data Description

Dr. Shuen-De Wu
August 15, 2014

Introduction

- Rolling bearing failure represents a high percentage of the breakdowns in rotating machinery and may result in catastrophic failures.
- Failure prognosis in long-term predictions are important topics when trying to ensure safety of the operation of machine tool.
- The main issue in prognosis is the ability to detect anomaly of bearing as early as possible.
- In this study, we propose a prognosis algorithm for rolling bearings based on multiscale entropy, permutation entropy and support vector data description.

Frequency Response of Bearing at Different Stages

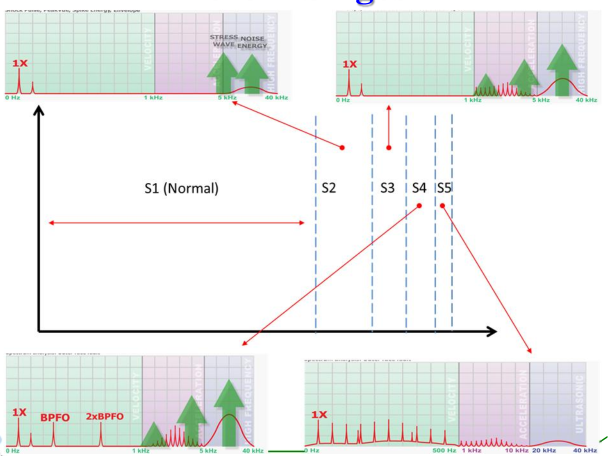

Anomaly Detection

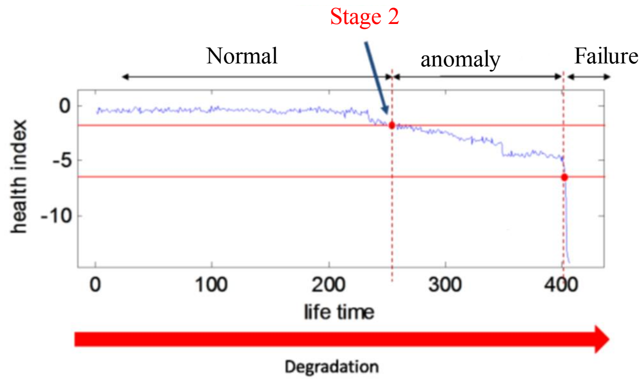

Proposed Algorithm

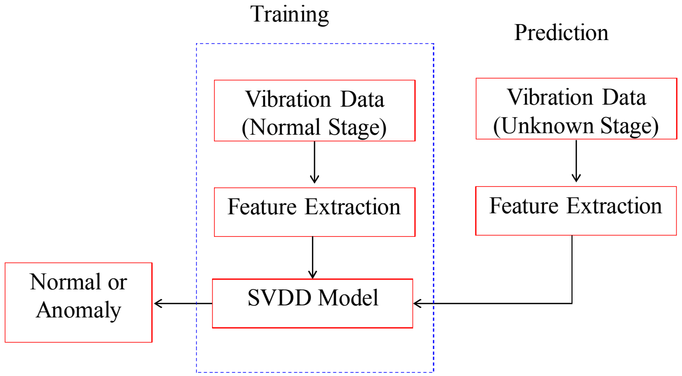

Sample Entropy

$m = 2$

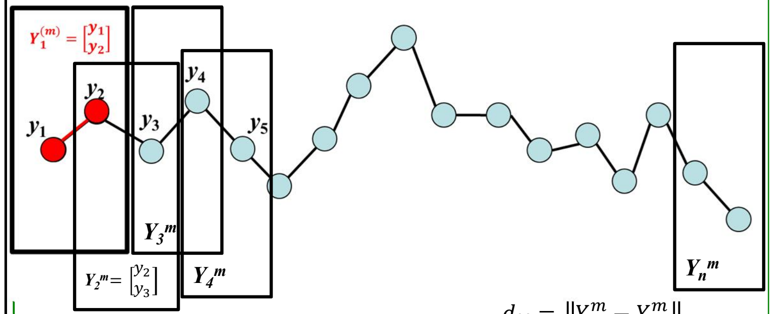

$d_{ij} = \|Y_i^m - Y_j^m\|_\infty$

if $d_{ij} < r$, $\varphi_m + 1$

r為0.15倍訊號標準差

Sample Entropy

$\varphi_m = 12$

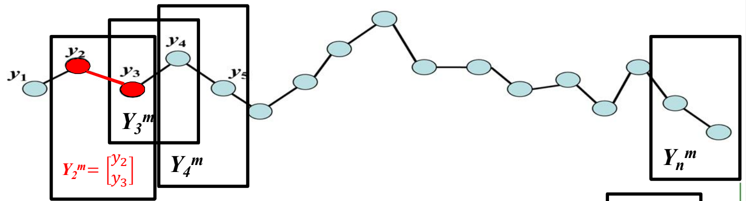

$\varphi_m = 40$

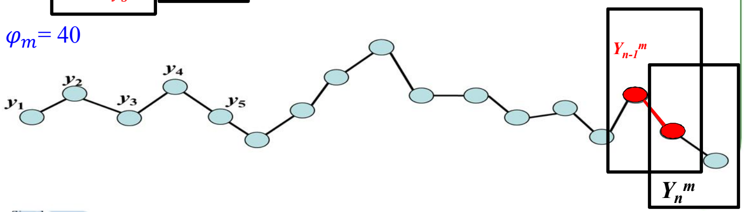

Sample Entropy

$\varphi_m = 11$

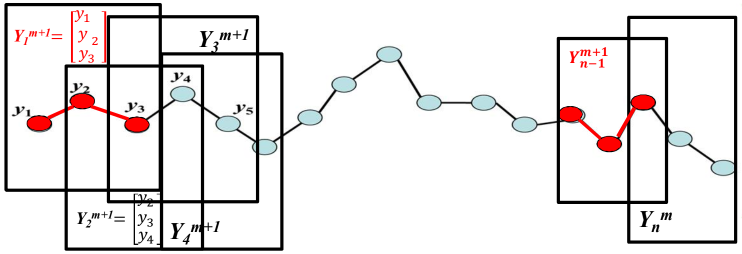

$$SE(m,r) = -ln\left(\frac{\varphi_{m+1}(r)}{\varphi_m(r)}\right) = -ln\frac{11}{40}$$

$d_{ij} = \|Y_i^{m+1} - Y_j^{m+1}\|_\infty$

if $d_{ij} < r$, $\varphi_{m+1} + 1$

Multiscale analysis

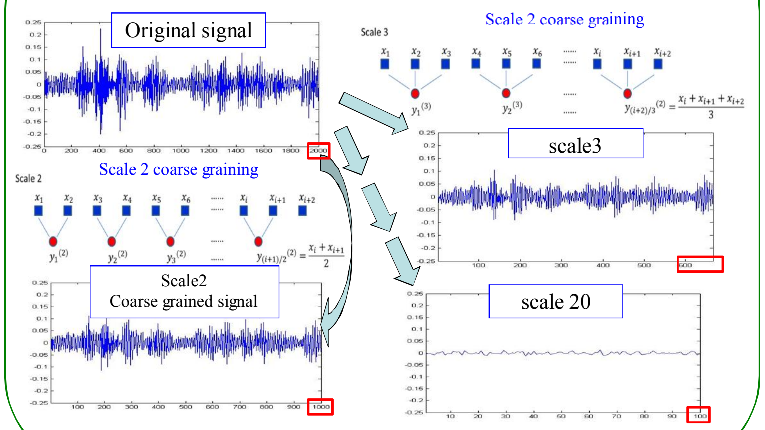

Multiscale Entropy Index

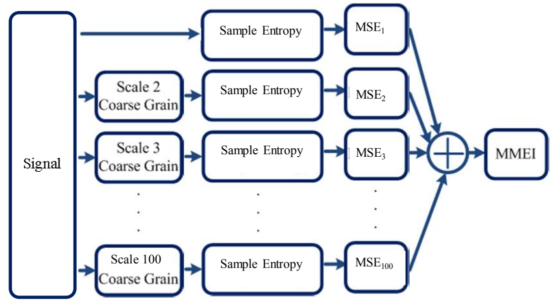

Permutation entropy

- **x**=(4,7,9,10,6,11,3) $m = 3$
- $$\begin{bmatrix} \mathbf{x}_1^3 \\ \mathbf{x}_2^3 \\ \mathbf{x}_3^3 \\ \mathbf{x}_4^3 \\ \mathbf{x}_5^3 \end{bmatrix} = \begin{array}{c} \begin{array}{ccc} 0 & 1 & 2 \end{array} \\ \begin{bmatrix} 4 & 7 & 9 \\ 7 & 9 & 10 \\ 9 & 10 & 6 \\ 10 & 6 & 11 \\ 6 & 11 & 3 \end{bmatrix} \end{array} \begin{array}{l} \leftarrow \pi_{012} \\ \leftarrow \pi_{012} \\ \leftarrow \pi_{201} \\ \leftarrow \pi_{102} \\ \leftarrow \pi_{201} \end{array}$$
- $p(\pi_{012}) = 2/5$, $p(\pi_{102}) = 1/5$, $p(\pi_{201}) = 2/5$
- $PEn(\mathbf{x}, 3)$ = -2/5ln(2/5) -1/5ln(1/5) -2/5ln(2/5) = 1.522
- Normalize: $nPEn(\mathbf{x}, 3) = \frac{1.522}{\ln(3!)} = 0.8494$

Support Vector Data Description

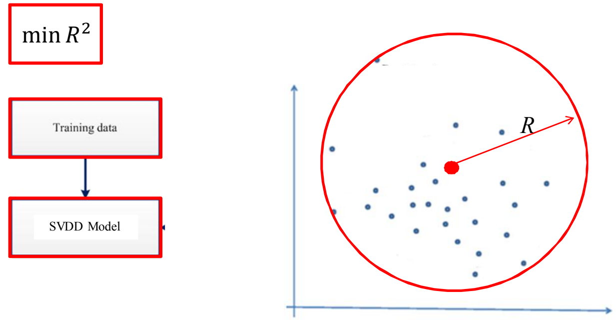

Support Vector Data Description

$\boxed{\min R^2}$

Testing Data

↓

SVDD Model

↓

1: Normal
-1: Anomaly

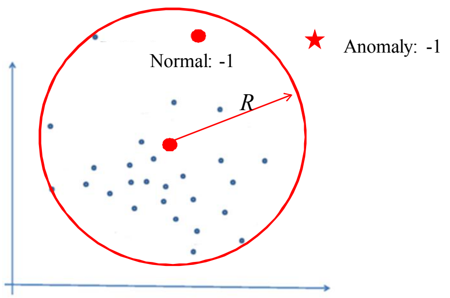

Support Vector Data Description

$\boxed{\min R^2}$

Anomaly may be classified as normal by SVDD when R is too large

Testing Data

↓

SVDD Model

↓

1: Normal
-1: Anomaly

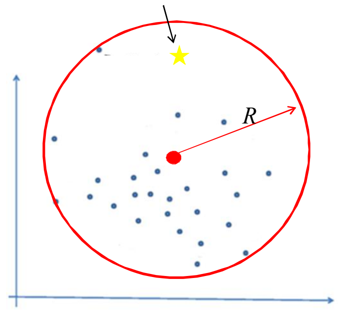

Support Vector Data Description

$\boxed{\min R^2} + \boxed{C \sum_i \xi_i}$

Training data

↓

SVDD Model

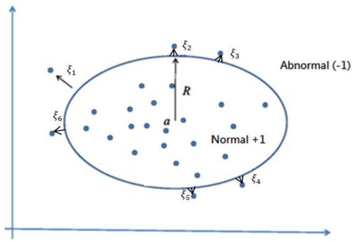

Support Vector Data Description

Kernel function: $k_G(\mathbf{x}_i, \mathbf{x}_j) = \exp\left(\frac{-(\mathbf{x}_i - \mathbf{x}_j)^2}{\boxed{2\sigma^2}}\right)$

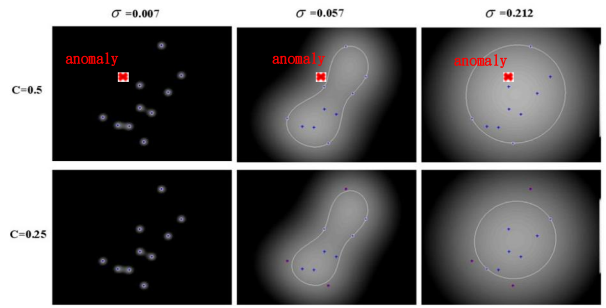

中原大學劉益宏碩士論文

Experimental Data

- IMS bearing Data
  - Motor speed : 2000 rpm
  - Load : 6000lb
  - Record : 1 sec / 10 min
  - Sampling rate : 20k Hz
  - Time : 164 hr
  - bearing 1 was damaged

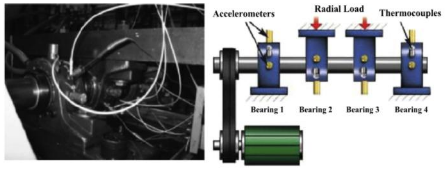

Past Approach

D. Fernandez-Francos, D. Martinez-Rego, O. Fontenla-Romero, and A. Alonso-Betanzos, "Automatic bearing fault diagnosis based on one-class v-SVM," Computers & Industrial Engineering, vol. 64, pp. 357-365, Jan 2013.

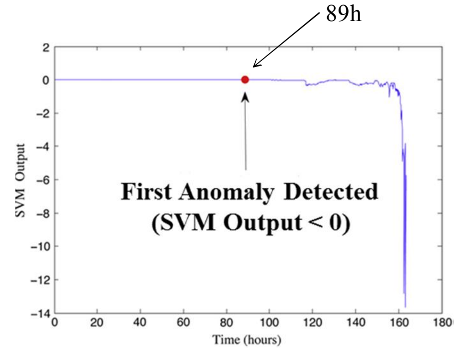

Past Approach

- Spectrum analysis of vibration data

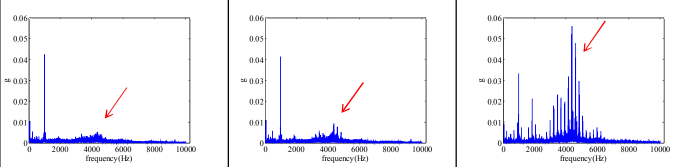

(a)Normal state(40h)	(b)Minor damage(89h)	(c)Serious damage(120h)

Algorithm 1

- Results
  - Anomaly can be detected by using MEI、PE at 89h after the beginning of experiments。
- Difficulty
  - What is the threshold to distinguish anomaly state form normal state?

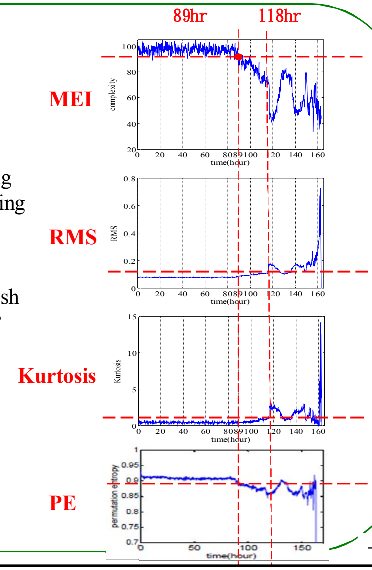

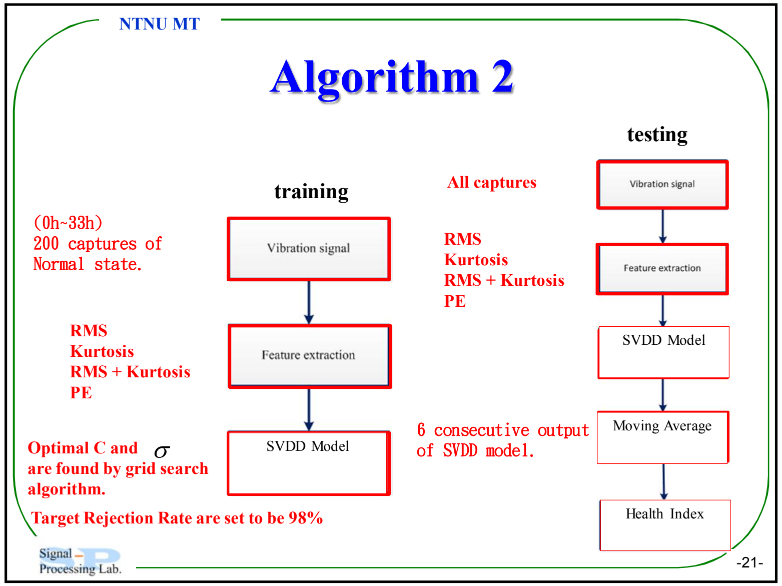
NTNU MT
Algorithm 2
training
testing
(0h~33h)
200 captures of
Normal state.
Vibration signal
Feature extraction
SVDD Model
RMS
Kurtosis
RMS + Kurtosis
PE
Optimal C and σ
are found by grid search
algorithm.
Target Rejection Rate are set to be 98%
All captures
RMS
Kurtosis
RMS + Kurtosis
PE
6 consecutive output
of SVDD model.
Vibration signal
Feature extraction
SVDD Model
Moving Average
Health Index
Signal Processing Lab.
-21-

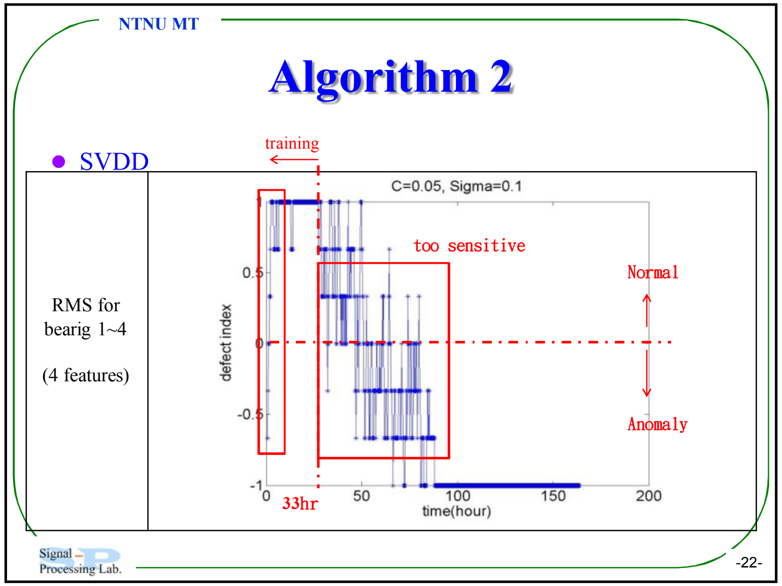
NTNU MT
Algorithm 2
SVDD
training
RMS for
bearig 1~4
(4 features)
C=0.05, Sigma=0.1
too sensitive
Normal
Anomaly
defect index
33hr
time(hour)
Signal Processing Lab.
-22-

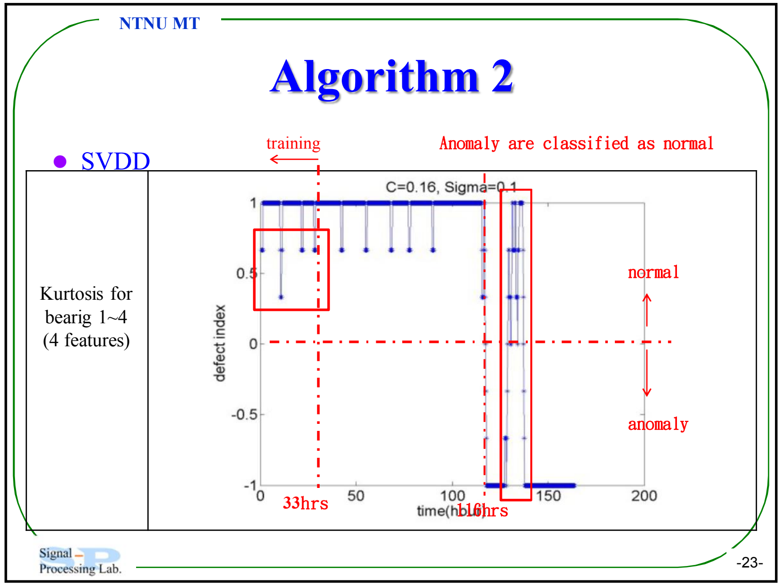
NTNU MT
Algorithm 2
SVDD
training
Anomaly are classified as normal
Kurtosis for
bearig 1~4
(4 features)
C=0.16, Sigma=0.1
normal
anomaly
defect index
33hrs
116hrs
time(hour)
Signal Processing Lab.
-23-

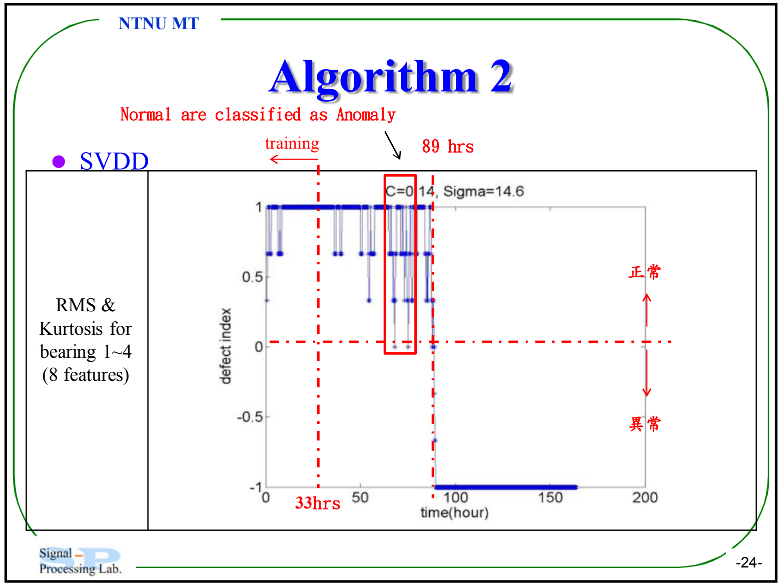
NTNU MT
Algorithm 2
Normal are classified as Anomaly
SVDD
training
89 hrs
RMS &
Kurtosis for
bearing 1~4
(8 features)
C=0.14, Sigma=14.6
正常
異常
defect index
33hrs
time(hour)
Signal Processing Lab.
-24-

Algorithm 2

- SVDD

PE for bearing 1~4 (4 features)	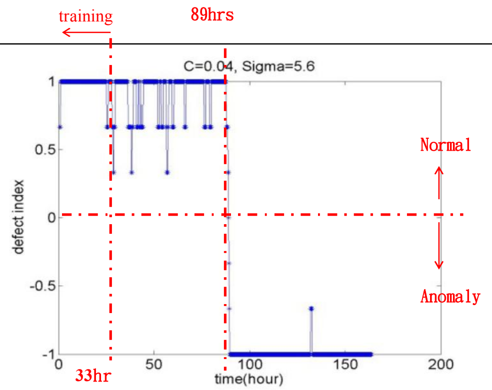

Conclusion

- Permutation entropy and Multiscale entropy seems to be a good index for the assessment of bearing performance degradation.
- Anomaly of bearing can be detected as early as possible by combing permutation entropy and support vector data description.

Q & A